Welding Colloidal Crystals with Carbon Dioxide

Howard Abramowitz, Parag S. Shah, Peter F. Green, and Keith P. Johnston*

Department of Chemical Engineering and Texas Materials Institute, University of Texas at Austin, Austin, Texas 78712

Received May 26, 2004; Revised Manuscript Received July 8, 2004

ABSTRACT: The effect of CO_2 on the welding kinetics for a PS colloidal crystal was determined by in-situ measurement of Bragg diffraction and by ex-situ SEM microscopy. The welds grow tangentially from the points of contact of the spheres in all directions transforming the spheres into a continuous film. The dissolved CO_2 provides the mobility for the polymer chains at the interface needed for welding, which removes the energetically unfavorable interfacial area between the polymer and CO_2. At high pressures where CO_2 is relatively incompressible, the relaxation time for welding increased by 6 orders of magnitude with an increase in thermal energy, and a glass transition temperature was observed. At constant temperature, an anomalous increase in the welding rate by 1−2 orders of magnitude with a decrease in pressure was observed in the region where CO_2 is highly compressible. It is likely that this increase in welding dynamics is influenced by the excess CO_2 in the interfacial region.

Introduction

The chemical potential of supercritical fluids including CO_2 is highly tunable with pressure and temperature and may be used to manipulate physical and chemical properties.[1] This tunability and excellent transport properties and interfacial properties are beneficial for processing polymers[2,3] and ordered metal nanoparticle films[4] while minimizing dewetting.[5] The prevention of dewetting is favored by greater control over the solvent chemical potential gradient during evaporation and the extremely low surface tension of liquid CO_2.[4] CO_2 is a nonflammable, essentially nontoxic, inexpensive, and environmentally benign solvent that is already used commercially in spray coating[6] Teflon production, polymer foaming, and dry cleaning to reduce emissions.[7] The low viscosity and surface tension may be exploited to generate extremely uniform thin films of photoresists on silicon wafers by spin-coating.[8] CO_2 is also of interest in lithographic processing of microelectronic devices with feature smaller than 100 nm,[7,9] drying of photoresists,[10,11] synthesis[3] and cleaning[7,12] of low-*k* dielectric films, polymer foaming, and membrane separations.[13,14] Suspensions of poly(2-ethylhexyl acrylate) in supercritical CO_2 were sprayed to form uniform films.[15] The viscosity reduction of the dispersed phase caused by dissolved CO_2 was required for atomization to produce fine droplets and for coalescence and leveling on the surface to form a uniform film.

Most polymers are not soluble in carbon dioxide, making them ideal candidates as matrices or templates for materials processing. Because CO_2 is a small and linear molecule, it diffuses into polymers faster than other swelling agents or plasticizers. The swelling and thus the mobility of the polymer chains may be fine-tuned by adjusting the CO_2 pressure, for example, in aqueous polystyrene latexes.[16] A local maximum in the swelling was observed near the critical point due to the large Gibbs excess adsorption that results from the high compressibility of CO_2. For polymer−CO_2 systems, the reduction in viscosity may be calculated as a function of the fractional free volumes of the pure polymer and polymer−supercritical fluid mixtures.[17,18] As CO_2 is added to a polymer by raising the pressure, the glass transition temperature decreases nearly linearly with the solubility of CO_2 in the films[19,20] and may be described with lattice−fluid theory and the Gibbs−Dimarzio criterion.[21] A reduction of the T_g by 70 °C at 100 atm is common. Once plasticized with CO_2, polymers become accessible and may be impregnated with dyes, pharmaceuticals, or organometallic precursors.[1,22,23] The diffusion constant of a typical organic molecule may increase several orders of magnitude.[24,25] After the CO_2 pressure is released the impregnated agent is trapped in a rigid glassy matrix. Pai et al.[3] have controlled the swelling of preordered block copolymer template films to allow the infusion of organic organometallic precursors. The catalyst only diffuses into the continuous phase block. Silicate is formed only in the continuous phase, resulting in a porous low dielectric constant insulator with excellent mechanical properties for use in microelectronics devices.

Recently, fundamental studies of properties of thin films exposed to CO_2 have been reported. The glass transition temperature of PS thin films decreases with film thickness as the contribution from the free surface containing excess CO_2 becomes increasingly important.[26,27] In systems without CO_2, the T_g is known to change as a function of depth from the free surface to the substrate based on fluorescent tags.[28] Neutron reflectivity studies of grafted chains on surfaces in CO_2 indicate that the volume fraction profiles are more sensitive to solvent quality than for chains in conventional liquids because of large differences in intermolecular interactions, compressibility, and free volume between chains and solvent.[29]

In regions where CO_2 is highly compressible, an anomalous maximum is observed in the adsorption of CO_2 on a hard surface, for example activated carbon.[30] This anomalous maximum has also been observed in the swelling of soft materials, for example 50 nm polystyrene latexes, as determined with dynamic light scattering.[16] For poly(methyl methacrylate films) (PMMA) thin films, the anomalous maximum in the swelling, which is not present in bulk films, was observed with in-situ ellipsometry.[31] The anomalous maximum was

* Corresponding author. E-mail: kpj@che.utexas.edu.

10.1021/ma048961b CCC: $27.50
Published on Web 08/27/2004

attributed to inhomogeneities in concentration at the free surface of the polymer[31] that may be expected to result from the large compressibility of CO_2.[1,32,33] This anomalous swelling phenomena was also observed with neutron reflectivity.[34,35] Furthermore, plasticization associated with the density fluctuations was shown to enhance polymer interdiffusion by 1 order of magnitude.

Herein we investigate the dynamics of welding photonic (colloidal) crystals of PS microspheres into uniform thin films by CO_2 with scanning electron microscope imaging (SEM) and in-situ optical measurements. Photonic crystals are materials that have a periodic refractive index in 3 dimensions. As theorized in 1987 by Yablonovitch[36] and John,[37] there exists a range of wavelengths in the electromagnetic spectrum that cannot propagate through these crystal in any direction. These wavelengths are referred to as a photonic band gap (PBG). The crystal structure creates the PBG which diffracts light in an analogous manner to atomic semiconductor crystals that diffract electrons.[38] A high refractive index difference is necessary to form a complete PBG; however, crystals with lower refractive index differences can exhibit a pseudo-band gap that partially blocks out a range of wavelengths.[39,40] The PS crystals fall in this range because the refractive index difference between PS (1.59) and the surroundings (air 1.003 or CO_2 1.04−1.22)[41] is not large enough to create a complete PBG. The location of the PBG is dependent on the refractive index of the materials and the lattice spacing and can be approximated by Bragg's law for diffraction

$$\lambda = \frac{2d_{hkl}}{m}\sqrt{(n_{avg}{}^2 - \sin^2(\theta))} \qquad (1)$$

Here λ is the central wavelength of the PBG and m is the order of the diffraction ($m = 1, 2, 3, ...$). The average refractive index is given by $n_{avg} = n_1\varphi_1 + n_2\varphi_2$, where φ_i is the volume fraction of the ith component (for a close packed lattice structure the occupied volume is 74%). The angle of incidence, θ, was 0° for these measurements as the incident beam was normal to the ⟨111⟩ plane. The interplanar spacing, d_{hkl}, changes depending on the lattice plane and for a cubic lattice is given by

$$d_{hkl} = \frac{a}{\sqrt{(h^2 + k^2 + l^2)}} = \frac{D\sqrt{2}}{\sqrt{(h^2 + k^2 + l^2)}} \qquad (2)$$

Here a is the lattice spacing and D is the particle diameter.[40] Combining eqs 1 and 2 and setting $\theta = 0$ gives

$$\lambda = \frac{2an_{avg}}{m\sqrt{(h^2 + k^2 + l^2)}} \qquad (3)$$

For first-order diffraction, the calculated PBG wavelength was 457 nm for the dominant ⟨111⟩ plane and 195 nm PS microspheres in air, which will be shown to agree with experimental results.

The objective of this study was to measure the dynamics of welding of photonic crystals with CO_2. The colloidal crystal is composed of multilayers of PS microspheres, allowing for the investigation of thin film properties in films that are several microns thick. This study is also the first to look at free-standing polymer thin film properties in CO_2. This is possible since only the bottom layer of the colloidal crystal is bound to the substrate. Complementary PBG measurements and SEM micrographs of the morphology are utilized to interpret the polymer dynamics in terms of interfacial driving forces, the glass transition, and polymer viscosity. The fusing of the colloidal crystal into a thin film causes the PBG to decrease in intensity due to a decrease in the periodicity of the refractive index. The polymer relaxation dynamics may be measured indirectly at various temperatures and pressures. This technique does not require a model, which is often required in other techniques such as ellipsometry. The increased mobility of the PS when in contact with CO_2 enhances the rate of relaxation of the colloidal crystal spheres. This relaxation is driven by the interfacial tension that exists between PS and CO_2 as well as Brownian motion of the PS chains, as has been shown for welding of dry acrylic latexes at ambient pressure.[42] The viscosity of the swollen polymer is estimated as a function of the CO_2 temperature and pressure in three distinct pressure regions. An unusual decrease in the relaxation time with a decrease in CO_2 pressure is observed in the highly compressible region. Given the developing photonic applications of colloidal crystals,[43,44] the ability to stabilize the crystals with small amounts of welding with CO_2 is of great practical interest.

Experimental Section

Colloidal Crystal Preparation. Colloidal crystals were prepared from an aqueous solution of sulfate stabilized polystyrene (PS) microspheres (Seradyn, lot # 1575). These particles were diluted in deionized water to ∼0.1 wt %. A 10 mm long by 8 mm wide glass microscope slide, cut to fit inside of a high-pressure cell described below, was cleaned with ethanol and deionized water. It was suspended vertically in the aqueous PS dispersion. The dispersion was placed inside a convection oven at ∼40 °C overnight, which allowed for a controlled rate of evaporation to produce higher quality crystals. The evaporation creates convective flow that forces the PS microspheres into the meniscus at the glass−water interface where they self-assemble on the glass slide into a close packed FCC structure (about 10−20 layers of spheres). The resulting crystals exhibit a PBG between 455 and 460 nm for different samples. According to eq 3 with a PBG at 457 nm, the calculated particle size was 195 nm. The particle size was also measured independently with both SEM images and dynamic light scattering, which gave particle sizes of 195 and 200 nm, respectively. The agreement validates the photonic band gap measurements.

UV−Vis Measurements. Photonic crystals were held vertically in the center of a high-pressure cell using a custom-made mount. The cell had two cylindrical sapphire windows (diameter = 2.54 cm and thickness = 0.95 cm) and a 0.9 cm optical path length. The cell was then placed in a Cary 3E UV−vis spectrophotometer and heated with heating tape. The temperature was monitored with a thermocouple inserted into a hole drilled in the side of the high-pressure cell. It was controlled to within ±0.2 °C. The cell was then pressurized with carbon dioxide (between 63.5 and 347 bar), using an ISCO 260 D syringe pump. Scans were taken at regular time intervals, as short as every 15 sec, and the change in the photonic band gap was monitored as a function of time at various conditions. Since each scan took a significant amount of time, typically 25 s, each time is reported as the time at the start of the scan. The scan time was reduced to about 10 s for the conditions where welding was the fastest, on the order of about 10 s.

Results and Discussion

Figure 1a shows an SEM image of a typical PS photonic crystal composed of 195 nm microspheres prior to exposure to CO_2. It can be seen that the particles self-

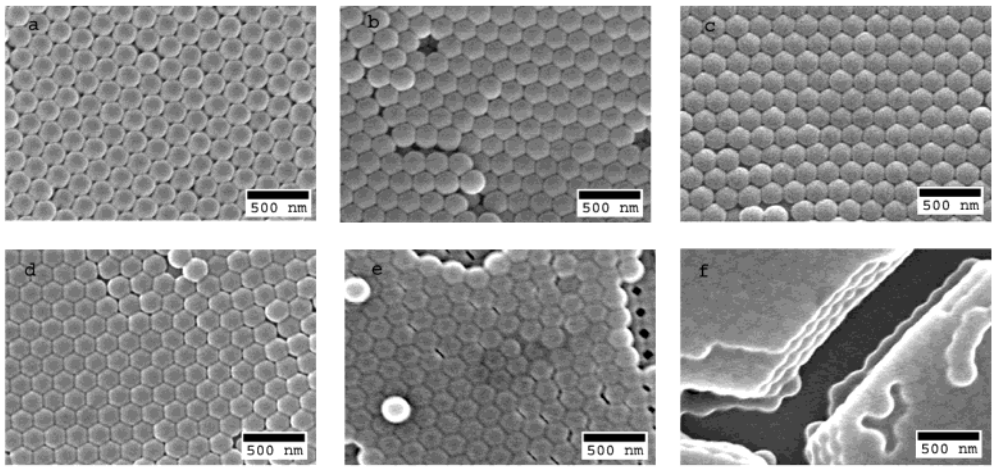

Figure 1. SEM micrographs of PS photonic crystals. (a) Unmodified crystal of PS self-assembled into an fcc lattice. (b−f) Various stages of the welding in CO_2 at 32 °C and 256 bar by varying the exposure time: (b) 6, (c) 15, (d) 70, (e) 120, and (f) 3600 min.

assemble into close packed lattices[43] with long-range order at the meniscus as the water evaporates. In Figure 1b−f the exposure time varies from 6 to 3600 min. In this series of images, the lattice spacing decreases as the PS welds together to form a nearly uniform film. Although it is difficult to see the welding in the direction normal to the substrate in this particular cleft in the SEM, it is present as will be apparent in the photonic band gap data below. At early times, 6 and 15 min, the microspheres are still almost spherical, as the PS spheres have only begun to weld together. Small necks have begun to form between adjacent particles. The welding begins where the two spheres are in contact. As time passes, the welds grow tangentially from this point of contact in all directions until they encompass the entire surface of the microspheres. They essentially "zip" together from each point of contact in 3 dimensions until a film is formed. For the particles, with the exception of the top layer, each sphere interacts with its 12 nearest neighbors. However, at the surface each sphere has only nine nearest-neighbor particles, and only the interactions between the six particles in the ⟨111⟩ plane are visible and appear as two-dimensional "hexagons" in the SEM images. The volume occupied by the welded particles, after depressurization to remove CO_2, should be similar to that of each sphere initially in the lattice. Since the CO_2 did not nucleate voids in the polymer, the polymer density after depressurization is the same as before the introduction of CO_2; thus, the volume of the polymer should be unchanged. The volume of the resulting structure can be approximated by a volume-filling model where the particles rearrange into pentagonal dodecahedra. This geometry is not completely void filling, but it has a void volume of only 3% and can approximate the change in lattice spacing seen in the SEM images. From the initial sphere size and assuming constant density the side-to-side length across the dodecahedron was calculated to be 177 nm. This agrees, within experimental error, with the end-to-end lengths found from the SEM micrographs of 174 nm after 120 min (where the lattice spacing no longer decreases).

The welding decreases the periodicity in the refractive index of the crystal, influencing both the peak height and the wavelength maximum. As shown in Figure 2, the photonic band gap shifts to the red (higher wavelengths) when the cell is first pressurized with CO_2 (at time $t = 0$). This shift is caused by two factors: the

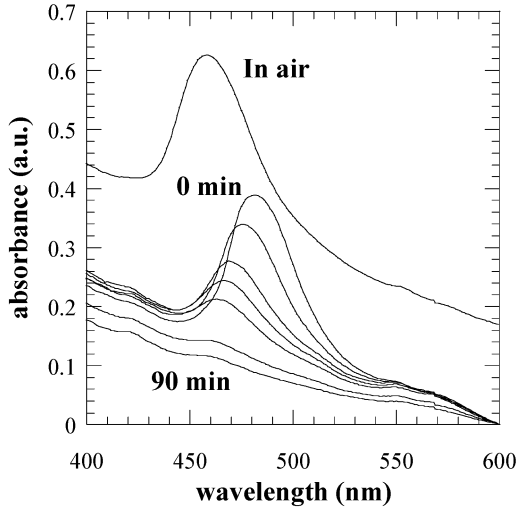

Figure 2. Photonic band gap of the colloidal crystals in air and under CO_2 at 35 °C and 89.6 bar at different times from 0 to 90 min. The times are shown in order for 0, 6, 15, 21, 30, 60, and 90 min. The PBG undergoes a blue shift as the lattice spacing decreases. The size of the PBG decreases as the periodicity of the refractive index disappears.

swelling of the polystyrene spheres by CO_2 and an increase in the continuous phase refractive index. The larger diameter of the swollen particles produces a red shift according to eq 3. In addition, the larger refractive index of CO_2 vs air increases the interstitial refractive index, which also causes a red shift. However, the decrease in the refractive index of the polystyrene when it is swollen with CO_2 limits the degree of the red shift. The refractive index of the CO_2−polymer mixture can be estimated from mixing rules for a binary liquid mixture.[45]

Figure 2 also shows that the peak shifts to the red upon first exposure and then begins to shift to the blue soon after exposure. This trend was consistent for all the scans performed. If the shift were dominated by swelling alone, it would continue to shift toward the red. The diffusion of CO_2 into the polymer spheres may be expected to take very little time according to the approximate equation $x \approx (D_{AB}t)^{1/2}$ for the diffusion of CO_2 into PS. The highest expected value for the CO_2−PS diffusivity, D_{AB}, was used (3.9×10^{-8} cm^2/s for amorphous atactic PS)[45] to solve for the time where the distance, x, was assumed to be 100 nm, approximately

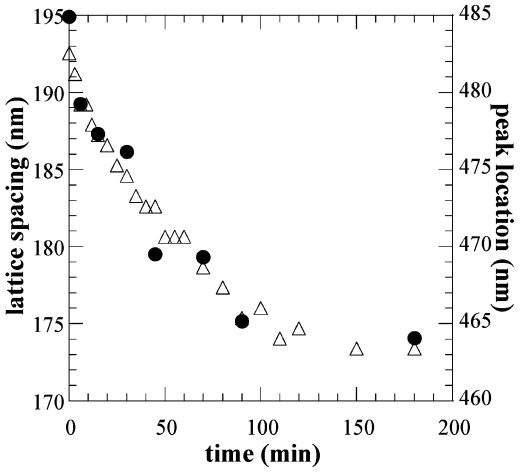

Figure 3. (●) Lattice spacing of the photonic crystal vs time under CO_2 at 32 °C and 256 bar calculated from SEM images similar to those in Figure 1. (△) Peak location of the PBG found from UV−vis absorption spectra at the same condition.

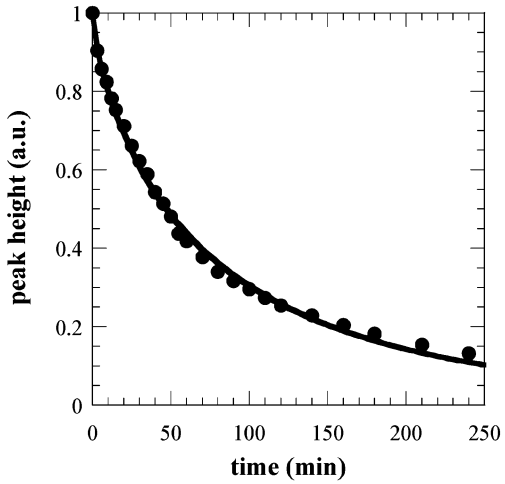

Figure 4. A typical peak height decay as the PS welds together at 32 °C and 187.9 bar.

the particle radius. The calculated time was 0.0026 s, which justifies the assumption that the particles were swollen completely with CO_2 upon pressurization before the scans began. Even if D_{AB} were 1000 times slower, the swelling would still be small relative to the scan time.

Qualitatively similar blue shifts have been observed during sintering of colloidal crystals of SiO_2. In these crystals the blue shift was caused by the viscous flow of the SiO_2 into the vacancies as the crystal was heated above its glass transition point.[46] Similarly, in our case the blue shift is the result of PS beads welding together and filling in the vacant space in the crystal lattice, reducing the size of the unit cell as is shown in Figure 1. This change in the Bragg diffraction peak is a measure of the reduction in the lattice spacing in the direction normal to the substrate.

In Figure 3, the lattice spacings from multiple samples cut out from the same photonic crystal were calculated from SEM images like those in Figure 1. The data point at $t = 0$ is prior to exposure to CO_2. Figure 3 also shows the change in peak position of the PBG vs time. The decreasing wavelengths mirror the decreasing lattice spacing, as would be expected from the equation for Bragg diffraction (eq 3) showing that the welds grow at the same rate in all directions.

The rate at which the PBG decayed was evaluated by monitoring the change in peak height, H (height of the absorbance peak minus the baseline), as a function of time at the various conditions. Figure 4 shows a typical plot of peak height vs time. To compare the various conditions, an exponential decay was fit to the points to determine a relaxation time τ as shown.

$$H = H_0 \exp(-(t/\tau)^n) \tag{4}$$

Here H_0 is the initial peak height of the band gap and n is an exponent to account for the shape of the decay.

The interfacial free energy, γA, is a driving force for welding of the mobile polymer chains in the spheres. The interfacial tension, γ, creates a stress on the large interfacial area, A, that is present in an array of spheres. The interfacial area decreases upon welding and decays to zero as a uniform film is formed. The simple model of Mackenzie and Shuttleworth has been shown to be successful for the description of dry sintering of methyl methacrylate and 2-ethylhexyl acrylate copolymer latexes.[42,47] It may be applied to interpret our data in CO_2. The kinetics of the removal of voids is approximated by a relationship for viscous flow driven by the interfacial energy at the polymer surface

$$\frac{dr}{dt} = -\frac{\gamma}{2\eta}\left(\frac{1}{\rho(r)}\right) \tag{5}$$

where dr/dt is the rate of change in the void space, approximated by spheres with a radius r, γ is the interfacial tension, η is the viscosity of the polymer dispersed phase, and $\rho(r)$ is the dimensionless density (film density divided by the density of a uniform thin film).[42,47] ($\rho(r)$ equals 0.74 for a close packed array of spheres and 1 for a uniform film.)

From the spectral data (see Figure 4), relaxation times were found at various temperatures and pressures. In cases where γ is essentially constant with a change in the CO_2 pressure or temperature, in eq 5, the relaxation time is proportional to the viscosity of the polymer:

$$\tau \sim \eta \sim \exp(E/k_b T) \tag{6}$$

where η is the viscosity of the polymer and E is an activation energy.[48] This relationship provides a correlation between the rate of decay in the PBG and the PS mobility, $1/\eta$, under various CO_2 conditions.

The results of these relaxation times regressed from eq 4 can be seen in Figures 5 and 6 where the relaxation time is plotted vs pressure and density at three different temperatures (32, 35, and 40 °C). Values of dr/dt were calculated from the rate of change in the location of the photonic band gap (Figure 7A), and γ values were approximated[49] (Figure 7B, see Appendix). Given dr/dt and γ, the viscosities of the CO_2 swollen polymer were calculated with eq 5. The results are shown in Figure 7B where mobility, $1/\eta$, is plotted versus density at constant temperature of 35 °C. Figure 7A shows a correspondence between the relaxation times and the rate of change in peak location, implying that both values are related to the change in lattice spacing in the photonic crystal.

From Figures 5 and 6 three pressure (or density) ranges of interest are observable: a high-pressure region, a compressible region at intermediate densities,

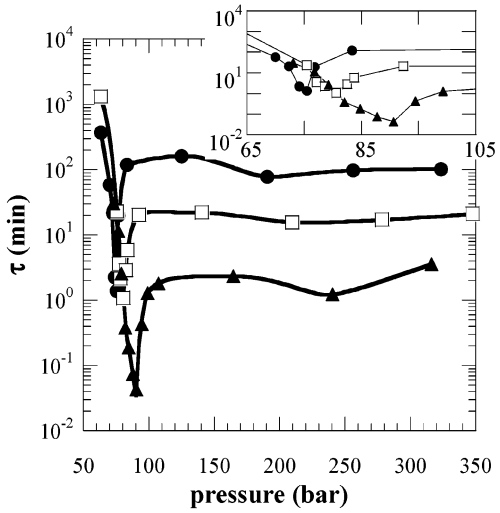

Figure 5. Relaxation time vs pressure: (●) 32, (□) 35, and (▲) 40 °C. The inset in the upper right focuses on the highly compressible region.

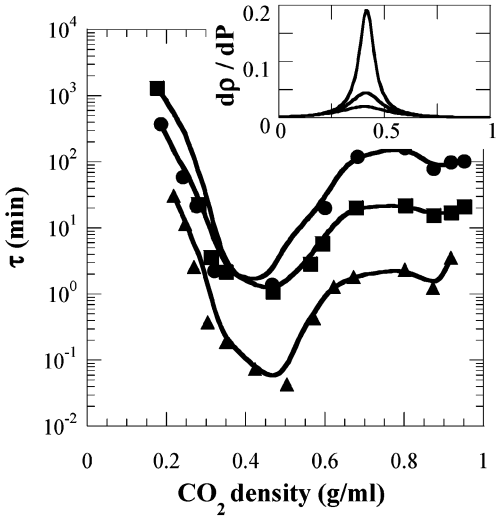

Figure 6. Relaxation time vs density: (●) 32, (■) 35, and (▲) 40 °C. In the inset the compressibility is plotted as dρ/dP as a function of CO_2 density using the Peng−Robinson equation of state. The largest peak corresponds to 32 °C, and the peaks decrease at 35 and 40 °C.

and a low-pressure region. These regions each have unique behavior that will define them as discussed below.

High-Pressure Region. A high-pressure plateau region is observed in Figures 5 and 6 to the right of each well for densities above 0.7 g/mL. Here the relaxation time is nearly constant with large changes in pressure or CO_2 density. This behavior may be examined with eq 5 after calculating γ. Figure 7B shows that γ, calculated from Hamaker constants approximated using Lifshitz theory,[49] is nearly linear in density. From eq 5, the combination of a plateau in relaxation times seen in Figures 5 and 6 and the decrease in interfacial tension with density implies a modest increase polymer mobility in this region, as shown for $1/\eta$ in Figure 7B.

The relaxation times were investigated for a variety of temperatures at a constant CO_2 density of 0.92 g/mL. Despite the small pressure effect on the relaxation time observed above, τ decreases 6 orders of magnitude with an increase in temperature of only 20 °C, as shown in Figure 8. The γ value for PS in air changes only slightly,

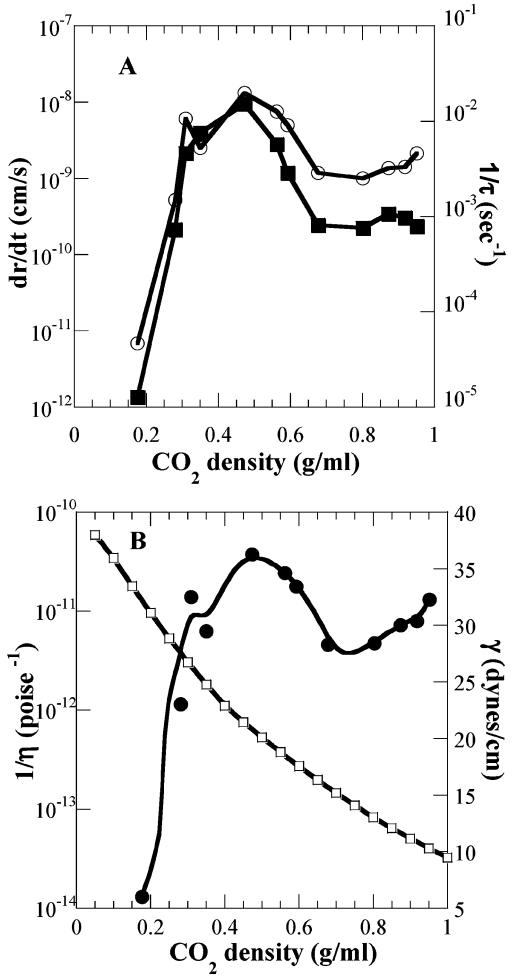

Figure 7. (A) Rate of change in void space of the crystal dr/dt (○) and the inverse of the relaxation time (■) plotted vs density at 35 °C. These two plots are very similar, which is expected from combining eqs 5 and 6. The viscosities were calculated using dr/dt. (B) Mobility (●), $1/\eta$, using dr/dt and the interfacial tension (□) which is also shown. In these graphs the values for γ were calculated as described in the Appendix.

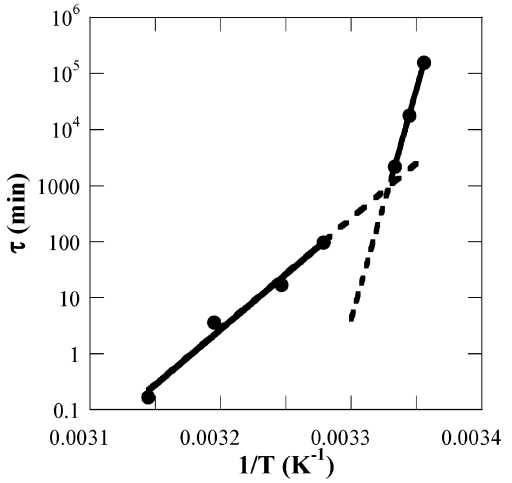

Figure 8. Relaxation time vs $1/T$ at constant CO_2 density (0.92 g/mL). The discontinuity in the relaxation time vs temperature curve is indicative of a glass transition at 27.5 °C.

from 40.3 to 38.9 dyn/cm, in this temperature range.[50] Similarly at constant CO_2 density, the temperature effect on the γ should also be negligible as predicted from the Hamaker constant.[49] The change in γ with

temperature is small relative to this enormous change in relaxation times. Thus, eqs 5 and 6 predict that the marked change in relaxation times are produced by the large increase in molecular mobility, that is, a large decrease in polymer viscosity with decreasing temperature.

In Figure 8 two linear regions are observed in the relaxation times, indicating a discontinuity in the molecular mobility. It is reasonable to attribute this change to a glass transition at 27.5 °C, a value similar to that found for bulk PS films under the same conditions in carbon dioxide.[51] These results imply that at high pressures the changes in relaxation time are a result of decreased viscosity due to an increase in thermal energy. In each region above and below the glass transition the exponential decay with k_bT indicates a thermally activated Arrhenius relationship, as predicted in eq 6. It is of note that the Arrhenius behavior in eq 6 does not describe polymer dynamics with changing temperature as accurately as the Williams−Landel−Ferry equation described below. However, for small temperature changes the Arrhenius relationship gives an accurate fit, as shown in Figure 8.

The activation energy in the less viscous rubbery region was found to be 378 and 1582 kJ/mol in the glassy region. The value for the activation energy in the rubbery region is larger than that observed by Gupta et al. at higher temperatures (62−85 °C) in CO_2 where an activation energy of 140 kJ/mol was found.[24] It is also larger than the activation energy of the melt at atmospheric conditions for temperatures above 100 °C, where Green et al. found the activation energy to be 254 kJ/mol for a molecular weight of 110 000 g/mol.[52] The differences between these two studies can be accounted for by the dependence of the activation energy on the presence of CO_2, which lowers segmental friction and increases the probability of critical void formation.[24]

The activation energy in this study is higher than the values found in the other studies because full liquid mobility is not present at the conditions studied. The data presented in this study are very close to the T_g value (27.5 °C), and in this range the polymer mobility is limited, as discussed in further detail below, and highly dependent on the temperature. The temperature dependence (activation energy) is greater than at higher temperatures, where a completely melted polymer phase exists. This temperature dependence can be accounted for by looking at a more accurate model of polymer dynamics, the Williams−Landel−Ferry equation[53]

$$\log\left(\frac{\tau}{\tau^*}\right) = \frac{-C_1(T - T^*)}{C_2 + (T - T^*)} \tag{7}$$

where C_1 and C_2 are constants with values of 12.5 and 50, respectively, for PS at 100 °C,[53] and τ^* is the relaxation time at the reference temperature T^*. Here the value for τ^* was the relaxation time at the glass transition (780 min). Fitting this model to the constant density data in the rubbery region gave values for C_1 and C_2 of 33.0 and 50.4, respectively. The T^* value was also found to be 301.9 K, which is essentially the same as the value for T_g found experimentally, 301 K. The value for C_1 varies significantly from the atmospheric value; however, the influence of CO_2 on the dynamics, as discussed above, could explain this discrepancy.

The final stage of welding in Figure 1f provides further evidence of the low mobility. The film exhibits residual surface structure and not a completely uniform film, despite the long welding time of 3600 min. As the chains overlap in the thin boundaries between particles, the interfacial area becomes small, decreasing the thermodynamic interfacial driving force for welding. Here Brownian motion becomes the main driving force for polymer mobility.

Low-Pressure Region. The low-pressure region is the area of Figure 5 where the relaxation times are longer than those found at the high-pressure plateau and go toward infinity with decreasing CO_2 pressure. This increase in relaxation time is expected as the amount of CO_2 sorption decreases markedly with decreasing pressure, and the polymer becomes very rigid as the P_g is approached.[31] However, the polymer microspheres still weld together very slowly at pressures slightly below the CO_2-induced bulk P_g found experimentally by Condo et al.[51] The 200 nm latex particles may be expected to exhibit thin film rather than bulk behavior. In the low-density region, the effects of surface mobility on the glass transition have been observed for polymer thin films exposed to CO_2.[26,27] The glass transition pressure of PMMA[26]and PS[27] thin films exposed to CO_2 decreases markedly as the film thickness is decreased from 100 to 15 nm. The high concentration of CO_2 at the surface provides more configurational mobility to the chain segments near the free surface at all pressures.

In addition, at ambient pressure, this mobile surface layer exists at temperatures near the T_g for PS films in air.[54] Another study has shown that PS films at temperatures 30 °C below the T_g still exhibit this mobility.[55] Results have shown that this phenomenon is independent of molecular weight, implying the mobility was driven by elastic relaxation of chain segments at the interface and not viscous flow of entire polymer chains.[55] The influence of the increased segmental motion of polymer chains due to surface mobility becomes more important as the film thickness decreases do to a loss of chain confinement relative to the bulk polymer.[28,56] Thus, a correlation has been found between the change in T_g and the free surface to volume ratio of the films.[57] Furthermore, the T_g is known to change as a function of depth from the free surface to the substrate based on fluorescent tags.[28]

The welding of the small spheres at conditions in the vicinity of the P_g may be expected to be facilitated by the existence of a mobile surface layer of the PS. Suppose that a mobile surface layer facilitates welding of the photonic crystals swollen by CO_2. A surface layer of ~9 nm would have to be mobile for 195 mm spheres to contract to 177 nm dodecahedra to remove the volume initially occupied by CO_2. This distance is comparable to the radius of gyration of the polymer. Mobile layers in air of this magnitude have been seen previously.

A driving force for welding in this region is the interfacial tension between the PS and the surroundings.[58] Figure 7B shows that interfacial tension of PS and CO_2 is significantly higher at low densities, below the critical density of CO_2 than in the high-density region. However, as CO_2 density is decreased, the effect of increasing γ is not able to overcome the loss of mobility due to decreased swelling and CO_2 sorption.[59] The loss of free volume in the polymer as a result of reduced sorption results in the increased viscosities seen in Figure 7B.[17] The shape of the curve of mobility vs density is similar to the shape of both the dr/dt and the

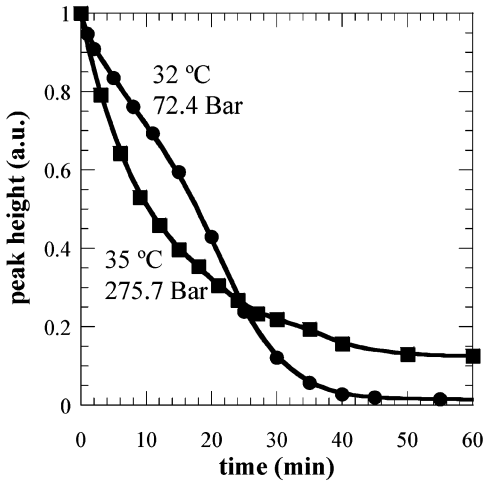

Figure 9. Comparison of shapes of the relaxation curves. The 72.4 bar curve shows a linear decay in the PBG with time in the low-pressure region while the 275.7 bar curve in the high-pressure region shows an exponential decay. Both curves have similar relaxation times 17 min at 35 °C and 21 min at 32 °C.

$1/\tau$ curves. The viscosities in this range were found from eq 6 to approach the viscosity of a glass (7.6×10^{13} P at 63.5 bar and 35 °C). A study of polymer welding at ambient pressure[55] found that flow is not caused by viscous flow of polymer chains in CO_2 but rather segmental motion of chain molecules at the surface of the polymer. This mechanism may be present in our study due to the large calculated viscosities in Figure 7B. Furthermore, the chains are not soluble in CO_2.

The decay of the photonic band gap also indicates differences in the mechanisms of welding in the high- and low-pressure regions. Figure 9 shows peak height vs time curves for two different state points with similar relaxation times. One condition was 35 °C and 275.7 bar (high-pressure region) while the other condition was at 32 °C and 72.4 bar (low-pressure region). The two curves have very different shapes, perhaps indicative of a change in the mechanism of polymer diffusion. Exponential decay was typically observed in our experiments in the high-pressure and compressible regions, as expected for classical particle diffusion from a ring source.[60] In the low-pressure region where PS spheres are quite rigid the typical decay was linear. The lack of bulk mobility may be the cause of the linear decay that deviates from the exponential decay that is seen for high pressures.

Highly Compressible Region. In this region between the high- and low-pressure regions, the compressibility of CO_2 is unusually large as shown in the inset of Figure 6. Here τ decreases reaches a minimum at about 0.45 g/mL and then increases. It is remarkable that τ decreased by over an order of magnitude beneath the plateau values in the high-pressure region of Figures 5 and 6. This unusual increase in the rate of welding was observed both in-situ in the PBG and with SEM micrographs of the films after depressurization. As the density is decreased from the high-pressure region to the highly compressible region, η^{-1} changes by an order of magnitude whereas γ only increases by a factor of about 2, as shown in Figure 7B (see also Figure 10b). Thus, this increase in welding rate is due primarily to an increase in polymer mobility and Brownian motion and only secondarily to the increase in γ. Even the removal of the residual surface features during the final stages of welding is rapid despite the low interfacial surface area and consequently the small free energy driving force, as shown in Figure 10.

Substrate−polymer interactions influence the T_g. Free-standing PS films have been shown to exhibit the same glass transition as films on a substrate with one-half the thickness.[57] In this study, only the bottom layer of the crystal is in contact with the substrate, and the other spheres are free-standing. Thus, the unusual behavior may not be attributed to a polymer substrate effect, consistent with the ellipsometric observations of Sirard et al.[31] for swelling of thin films.

Sirard et al.[31] proposed that these excess layers are also present on the surface of soft PMMA thin films and produce the anomalous peak in swelling in the highly compressible region. The thickness of the excess region due to density fluctuations is unknown for soft surfaces like polymers, but it may possibly penetrate several nanometers to tens of nanometers into thin films. For very thin films, the excess region may possibly penetrate through the entire film. This excess swelling would act to increase the free volume of the polymer chains as well as their overall mobility.[17]

The magnitude of the surface excess of CO_2 could influence polymer dynamics given its influence on the glass transition of a thin film. The surface excess of CO_2 on a hard impenetrable surface becomes extremely large in the critical region of pure CO_2 where the compressibility is large.[30,61] The mass of the excess layer follows the same trends as the size of the density fluctuations that are related to the isothermal compressibility.[61] The shape of the excess CO_2 vs pressure plot for hard surfaces is similar to that of the isothermal compressibility, $d\rho/dP$, shown in the inset of Figure 6. The shapes of the anomalous peaks seen in Figures 5 and 6 are similar to that of the isothermal compressibility, implying that the excess CO_2 in the interfacial region may possibly play a significant role in the anomalous increase in the rate of welding. The welding starts at the points of contact and moving tangentially along the spheres to zip them together to form a continuous film. The gap is very thin, and the high excess CO_2 concentration in the chains near the surface may add surface mobility to raise the rate of welding.

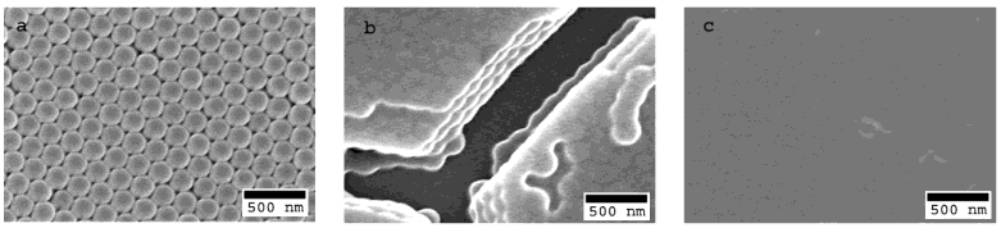

Figure 10. Welding in the high-pressure and highly compressible intermediate pressure regions. (a) Typical untreated PS photonic crystal image. (b) Welding of a photonic crystal in the high-pressure region at 32 °C and 256 bar for 3600 min. (c) Rapid welding in only 10 min at 32 °C and 71 bar in the highly compressible region.

Koga et al. used neutron reflectivity to study the interdiffusion of polymer between two thin films exposed to CO_2. The diffusion coefficient D_{AB} increased by 1 order of magnitude as the pressure was reduced from 70 to 13 MPa in the high-pressure incompressible region. As the pressure was further decreased to approximately 9 MPa, D_{AB} increased rapidly another order of magnitude in the highly compressible region. This increase in the highly compressible region was attributed to plasticization by CO_2 related to the anomalous swelling, as has been seen in our study. However, in the high-pressure incompressible region above 13 MPa, the compressibility was small, and thus it was unlikely that their nearly linear increase in D_{AB} was driven primarily by density fluctuations. Over this pressure range the swelling was relatively constant, again suggesting that density fluctuations were not important. In view of their large change in D_{AB} in the incompressible region, as well as our change in Figure 8 of 6 orders of magnitude as a function of temperature, it is apparent that other factors besides anomalous swelling, namely thermal energy and, to a smaller extent, interfacial tension, influence polymer dynamics.

Conclusions

The effect of CO_2 on the welding kinetics for a free-standing PS colloidal crystal was determined by in-situ measurement of Bragg diffraction and by ex-situ SEM microscopy. At high pressures where CO_2 is relatively incompressible, the relaxation time for welding increased by 6 orders of magnitude with an increase in thermal energy, and a glass transition temperature was observed. At constant temperature, an anomalous increase in the welding rate by 1−2 orders of magnitude with a decrease in pressure was observed in the region where CO_2 is highly compressible. This increase in welding dynamics is likely due to excess CO_2 in the interfacial region that increases polymer mobility and only secondarily to an increase in interfacial tension. This excess CO_2 in the highly compressible region has been observed in an anomalous swelling peak[31] and contributes to an anomalous increase in the diffusion of polymer between two thin films.[34] Not only is welding of colloidal crystals an efficient method for studying polymer diffusion at CO_2 interfaces, but CO_2 plasticization is of interest for welding and impregnation of colloidal crystals of interest in photonics applications. Furthermore, the ability to tune the degree of welding by controlling the pressure and temperature of CO_2 affords great control of the final morphology of the stabilized colloidal crystals, and no residual solvent is left in the product.

Acknowledgment. This work was supported by the STC program of the NSF under Agreement CHE-9876674, the Robert A. Welch Foundation, and the Separations Research Program at the University of Texas.

Appendix

To calculate the viscosities of the polymer using eq 5, values for the interfacial tension were needed. These values were approximated using a simplification of Lifshitz theory to approximate a Hamaker constant, A_{yy}, for a pure substance such that[62]

$$A_{yy} = \frac{3}{4}k_B T\left(\frac{\epsilon_y - \epsilon_{vacuum}}{\epsilon_y + \epsilon_{vacuum}}\right)^2 + \frac{3h\nu_e}{16\sqrt{2}}\frac{(n_y^2 - n_{vacuum}^2)^2}{(n_y^2 + n_{vacuum}^2)^{3/2}} \quad \text{(A1)}$$

where ν_e is the maximum electronic ultraviolet adsorption frequency, typically in the range $(3-5) \times 10^{15}$ s^{-1},[62] and is often assumed to be 3×10^{15} s^{-1}.[63] The values for the refractive index and dielectric of carbon dioxide were taken from the literature,[64] and for pure PS the values of the refractive index and the dielectric constant were 1.59 and 2.55,[62] respectively. However, in CO_2 the polymer becomes swollen with CO_2, and a simple volume fraction mixing rule was used to approximate these properties. The amount of swelling of PS with CO_2 was approximated from the values of Chang et al. The Hamaker constant for PS interacting with PS across CO_2 was approximated from the following relationship:[62]

$$A_{121} = (\sqrt{A_{11}} - \sqrt{A_{22}})^2 \quad \text{(A2)}$$

where A_{11} and A_{22} are the Hamaker constants for polystyrene and CO_2, respectively. From this calculated Hamaker constant a value for the interfacial tension can be calculated:[62]

$$\gamma = \frac{A_{121}}{24\pi D_0^2} \quad \text{(A3)}$$

D_0 is the interfacial contact separation, which is approximated as 0.165 nm.[62]

To solve for the viscosity using eq 5, dr/dt must first be determined. This was done by differentiating the equation for Bragg diffraction, eq 3, with time. In doing so, the average refractive index was assumed constant, and the particle radius was the only variable that changed with time. The actual change in the magnitude of n was small. The change in n between an initial array of PS spheres in air and a uniform film of is only ∼0.15; thus, its influence on dr/dt is negligible. From eqs 1 and 2

$$\frac{d\lambda}{dt} = \frac{dR}{dt}\frac{4\sqrt{2}}{\sqrt{3}}n_{avg} \quad \text{(A4)}$$

dλ/dt was approximated, for the initial welding of the crystal, by fitting a line to the first few peak location vs time values at each state point. From this dR/dt was approximated. However, eq 5 is expressed in terms of the void radius, which was found by inscribing a sphere into the vacant space between the crystals in the fcc lattice. The geometric relationship between the radius of the inscribed sphere and particle radius is given by

$$r = R(\sec(30°) - 1) \quad \text{(A5)}$$

Using this result in eq A4 and solving for dr/dt gives

$$\frac{dr}{dt} = \frac{d\lambda}{dt}\frac{4\sqrt{3}}{\sqrt{2}(\sec(30°) - 1)n_{avg}} \quad \text{(A6)}$$

It was assumed that the initial rate of void closure was constant (dλ/dt is constant), and for the initial welding,

$\rho(r)$ was assumed to be 0.74. Given eq A6, eq 5 was solved for the mobilities shown in Figure 7B. It is also of note that relaxation times could also be used to solve for viscosities by correlating the relaxation times with the rate of change in void space by combining eqs 5 and 6. Figure 7A shows good correlation between the values of τ and dr/dt.

References and Notes

(1) Eckert, C. A.; Knutson, B. L.; Debenedetti, P. G. *Nature (London)* **1996**, *383*, 313−318.
(2) Novick, B. J. D.; Joseph, M.; Carbonell, R. G. *Ind. Eng. Chem. Res.* **2004**, *43*, 515−524.
(3) Pai, R. A. H. R.; Schulberg, M. T.; Sengupta, A.; Sun, J.-N.; Watkins, J. J. *Science* **2004**, *303*, 507−511.
(4) Shah, P. S.; Novick, B. J.; Hwang, H. S.; Lim, K. T.; Carbonell, R. G.; Johnston, K. P.; Korgel, B. A. *Nano Lett.*, **2003**, *3*, 1671−1675.
(5) Johnston, K. P.; Shah, P. S. *Science* **2004**, *303*, 482−483.
(6) Nielsen, K. A. B.; D. C.; Glancy, C. W.; Hoy, K. L.; Kuo, A. C.; Lee, C. *Polym. Mater. Sci. Eng.* **1990**, *63*, 996−999.
(7) DeSimone, J. M. *Science* **2002**, *297*, 799−803.
(8) Hoggan, E. N. F. D.; DeSimone, J. M.; Carbonell, R. G. *Proceedings of SPIE−The International Society for Optical Engineering (Pt. 2, Advances in Resist Technology and Processing XIX)* **2002**, 1217−1223.
(9) Sundararajan, N.; Yang, S.; Ogino, K.; Valiyaveettil, S.; Wang, J.; Zhou, X.; Ober, C. K.; Obendorf, S. K.; Allen, R. D. *Chem. Mater.* **2000**, *12*, 41−48.
(10) Goldfarb, D. L.; Pablo, J. J. D.; Nealey, P. F.; Simons, J. P.; Moreau, W. M.; Angelopoulos, M. *J. Vac. Sci. Technol. B* **2000**, *18*, 3313−3317.
(11) Zhang, X.; Pham, J. Q.; Ryza, N.; Green, P. F.; Johnston, K. P. Submitted to *J. Vac. Sci. Technol., B* **2004**, *22*, 818−825.
(12) Zhang, X.; Pham, J. Q.; Martinez, H. J.; Wolf, J. P.; Green, P. F.; Johnston, K. P. Submitted to *J. Vac. Sci. Techol., B* **2003**, *21*, 2590−2598.
(13) Wind, J. D.; Sirard, S. M.; Paul, D. R.; Green, P. F.; Johnston, K. P.; Koros, W. J. *Macromolecules* **2003**, *36*, 6442−6448.
(14) Wind, J. D.; Sirard, S. M.; Paul, D. R.; Green, P. F.; Johnston, K. P.; Koros, W. J. *Macromolecules* **2003**, *36*, 6433−6441.
(15) Shim, J.-J.; Yates, M. Z.; Johnston, K. P. *Ind. Eng. Chem. Res.* **1999**, *38*, 3655−3662.
(16) Otake, K.; Webber, S. E.; Munk, P.; Johnston, K. P. *Langmuir* **1997**, *13*, 3047−3051.
(17) Gerhardt, L. J.; Manke, C. W.; Gulari, E. *J. Polym. Sci., Part B: Polym. Phys.* **1996**, 523−534.
(18) Kwang, C.; Manke, C. W.; Gulari, E. J. *J. Polym. Sci., Part B: Polym. Phys.* **1999**, *37*, 2771−2781.
(19) Chiou, J. S.; Barlow, J. W.; Paul, D. R. *J. Appl. Polym. Sci.* **1985**, *30*, 2633−2642.
(20) Wissinger, R. G.; Paulaitis, M. E. *J. Polym. Sci., Part B: Polym. Phys.* **1987**, *25*, 2497−2510.
(21) Condo, P. D.; Sanchez, I. C.; Panayiotou, C. G.; Johnston, K. P. *Macromolecules* **1992**, *25*, 6119−6127.
(22) Kazarian, S. G.; Vincent, M. F.; Bright, F. V.; Liotta, C. L.; Eckert, C. A. *J. Am. Chem. Soc.* **1996**, *118*, 1729−1736.
(23) Yates, M. Z.; Birnbaum, E. R.; McCleskey, T. M. *Langmuir* **2000**, *16*, 4757−4760.
(24) Gupta, R. R. R.; Vijayakumar, S.; Watkins, J. J. *Macromolecules* **2003**, *36*, 1295−1303.
(25) Cao, T.; Johnston, K. P.; Webber, S. E. *Macromolecules* **2004**, *37*, 1897−1902.
(26) Pham, J. Q.; Sirard, S. M.; Johnston, K. P.; Green, P. F. *Phys. Rev. Lett.* **2003**, *91*, 175503/175501−175503/175504.
(27) Pham, J. Q.; Johnston, K. P.; Green, P. F. *J. Phys. Chem. B* **2004**, *108*, 3457−3461.
(28) Ellison, C. J.; Torkelson, J. M. *Nature Mater.* **2003**, *2*, 695−700.
(29) Sirard, S. M.; Gupta, R. R.; Russell, T. P.; Watkins, J. J.; Green, P. F.; Johnston, K. P. *Macromolecules* **2003**, *36*, 3365−3373.
(30) Humayun, R. T.; David, L. *AIChE J.* **2000**, *46*, 2065−2075.
(31) Sirard, S. M.; Ziegler, K. J.; Sanchez, I. C.; Green, P. F.; Johnston, K. P. *Macromolecules* **2002**, *35*, 1928−1935.
(32) Brennecke, J. F.; Chateauneuf, J. E. *Chem. Rev.* **1999**, *99*, 433−452.
(33) Tucker, S. C. *Chem. Rev.* **1999**, *99*, 391−418.
(34) Koga, T.; Seo, Y.-S.; Hu, X.; Shin, K.; Zhang, Y.; Rafailovich, M. H.; Sokolov, J. C.; Chu, B.; Satija, S. K. *Europhys. Lett.* **2002**, *60*, 559−565.
(35) Koga, T.; Seo, Y.-S.; Zhang, Y.; Shin, K.; Kusano, K.; Nishikawa, K.; Rafailovich, M. H.; Sokolov, J.; Chu, B.; Peiffer, D.; Occhiogrosso, R.; Satija, S. K. *Phys. Rev. Lett.* **2002**, *89*.
(36) Yablonovitch, E. *Phys. Rev. Lett.* **1987**, *58*, 2059−2062.
(37) John, S. *Phys. Rev. Lett.* **1987**, *58*, 2486-2489.
(38) Yablonovitch, E. *J. Opt. Soc. Am. B* **1993**, *10*, 283−295.
(39) Joannopoulos, J. D.; Villeneuve, P. R.; Fan, S. *Nature (London)* **1997**, *386*, 143−149.
(40) Schroden, R. C.; Al-Daous, M.; Blanford, C. F.; Stein, A. *Chem. Mater.* **2002**, *14*, 3305−3315.
(41) Lewis, J. E.; Biswas, R.; Robinson, A. G.; Maroncelli, M. *J. Phys. Chem. B* **2001**, *105*, 3306−3318.
(42) Keddie, J. L.; Meredith, P.; Jones, R. A. L.; Donald, A. M. *Langmuir* **1996**, *12*, 3793−3801.
(43) Velev, O. D.; Jede, T. A.; Lobo, R. F.; Lenhoff, A. M. *Nature (London)* **1997**, *389*, 447−448.
(44) Velev, O. D.; Lenhoff, A. M.; Kaler, E. W. *Science* **2000**, *287*, 2240−2243.
(45) Tasic, A. Z.; Djordjevic, B. D.; Grozdanic, D. K. *J. Chem. Eng. Data* **1992**, *37*, 310−313.
(46) Miguez, H.; Meseguer, F.; Lopez, C.; Blanco, A.; Moya, J. S.; Requena, J.; Mifsud, A.; Fornes, V. *Adv. Mater.* **1998**, *10*, 480−483.
(47) Mackenzie, J. K.; Shuttleworth, R. *Proc. Phys. Soc.* **1949**, *62*, 833.
(48) Mezzenga, R.; Ruokolainen, J.; Hexemer, A. *Langmuir* **2003**, *19*, 8144−8147.
(49) Israelachvili, J. N. *Intermolecular and Surface Forces*, 2nd ed.; Academic Press: New York, 1992.
(50) Brandrup, J.; Immergut, E. H. *Polymer Handbook*, 3rd ed.; Wiley-Intersciences: New York, 1989.
(51) Condo, P. D.; Paul, D. R.; Johnston, K. P. *Macromolecules* **1994**, *27*, 365−371.
(52) Green, P. F.; Kramer, E. J. *J. Mater. Res.* **1986**, 202−204.
(53) Ferry, J. D. *Viscoelastic Properties of Polymers*, 3rd ed.; John Wiley and Sons: New York, 1980.
(54) Teichroeb, J. H.; Forrest, J. A. *Phys. Rev. Lett.* **2003**, *91*.
(55) Pu, Y.; White, H.; Rafailovich, M. H.; Sokolov, J.; Schwarz, S. A.; Dhinojwala, A.; Agra, D. M. G.; Kumar, S. *Macromolecules* **2001**, *34*, 4972−4977.
(56) Ngai, K. L.; Rizos, A. K.; Plazek, D. J. *J. Non-Cryst. Solids* **1998**, *235−237*, 435−443.
(57) Forrest, J. A.; Dalnoki-Veress, K. *Adv. Colloid Interface Sci.* **2001**, *94*, 167−196.
(58) Kerle, T.; Lin, Z.; Kim, H.; Russell, T. P. *Macromolecules* **2001**, *34*, 3484−3492.
(59) Zhang, Y.; Gangwani, K. K.; Lemert, R. M. *J. Supercrit. Fluids* **1997**, *11*, 115−134.
(60) Glicksman, M. E. *Diffusion in Solids*; John Wiley and Sons: New York, 2000.
(61) Giovanni, O. D.; Dorfler, W.; Mazzotti, M.; Morbidelli, M. *Langmuir* **2001**, *17*, 4316−4321.
(62) Israelachvili, J. N. *Intermolecular and Surface Forces*, 2nd ed.; Academic Press: New York, 1992.
(63) Dickson, J. L.; Ortiz-Estradan, C.; Alvarado, J. F.; Hwang, H. S.; Sanchez, I. C.; Luna-Barcenas, G.; Lim, K. T.; Johnston, K. P. *J. Colloid Interface Sci.* **2004**, *272*, 444−456.
(64) Lewis, J. E.; Biswas, R.; Robinson, A. G.; Maroncelli, M. *J. Phys. Chem. B* **2001**, *105*, 3306−3318.

MA048961B